Int J Fract (2007) 145:159–165
DOI 10.1007/s10704-007-9113-2

ORIGINAL PAPER

Edge chipping of brittle materials: effect of side-wall inclination and loading angle

Herzl Chai · Brian R. Lawn

Received: 3 May 2007 / Accepted: 9 August 2007 / Published online: 12 September 2007

Abstract An earlier analysis of chipping fracture in brittle solids is here extended to include the case of blocks with inclined side faces and non-normal contact loading. The simple relation $P_F = \beta K_c h^{3/2}$ for the critical chipping load P_F in terms of indent location h and material toughness K_c is preserved, with angular coordinates simply incorporated into the β coefficient. Chipping fracture tests using a Vickers indenter near the edges of glass blocks with non-orthogonal faces is used to validate the analysis. Implications of the results in relation to practical engineering, biomechanical and anthropological structures are indicated.

Keywords Vickers indentation · Inclined loading · Angular coordinates · Brittle ceramics · Edge chipping · Toughness

1 Introduction

Chipping from concentrated overloads is important in many areas: edge integrity in structural materials (masonry corners, ceramic tiles, kitchen crockery and countertops), edge-mounted optical lenses, small-scale devices (semiconductor chips, MEMS), material removal in ceramic machining, archaeological stone-tool knapping, survival of dental crowns in occlusal function. A considerable body of work on chipping fracture has been reported (McCormick 1982; Cotterell et al. 1985; Almond and McCormick 1986; Thouless et al. 1987; Lardner et al. 1990; Chui et al. 1998; Quinn et al. 2000; Morrell and Gant 2001; Morrell 2005; Scieszka 2005), but with little attempt to formulate critical loads P_F explicitly in terms of basic geometric and material properties. In a recent paper (Chai and Lawn 2007), using a simple geometrical similarity argument, we were able to derive such a relation for block specimens with orthogonal edge faces in normal loading at the top surface with a sharp-point contact:

$$P_F/h^{3/2} = \beta K_c \tag{1}$$

where h is the distance of the contact from the specimen edge, K_c is the toughness and β is a coefficient. Validation of this relation was carried out using Vickers indenters to induce edge chipping in glass and several ceramics. Apart from providing a basic underpinning of the mechanics of chipping fracture, Eq. 1 affords a simple route to toughness evaluation in fine-grain materials (Chai and Lawn 2007).

However, in reality many chipping configurations are more complex than the ideal geometry considered in the preceding studies. In particular, there may be angular components in the specimen and loading configurations. It is our goal in the present paper to

H. Chai
School of Mechanical Engineering, Faculty of Engineering, Tel Aviv University, Tel Aviv, Israel

B. R. Lawn (✉)
Materials Science and Engineering Laboratory, National Institute of Standards and Technology, Gaithersburg, MD, 20899-8520 USA
e-mail: brian.lawn@nist.gov

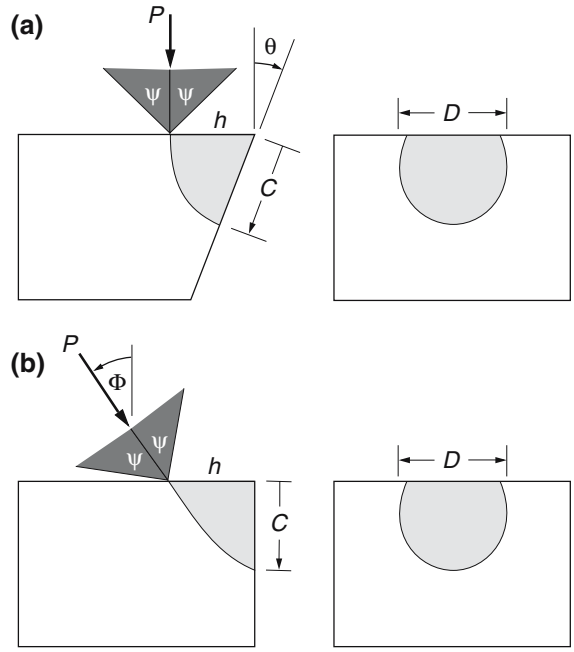

Fig. 1 Schematic showing (**a**) normal loading on blocks with inclined faces ($\theta \neq 0$), and (**b**) off-axis loading ($\phi \neq 0$) on rectangular blocks. Angles positive as drawn

generalize Eq. 1 to include such components. A special case is a non-orthogonal angle θ between faces adjoining the specimen edge (Fig. 1a). Another special case is a non-normal angle ϕ between load axis and specimen surface normal (Fig. 1b). Little has been done to establish the roles of these angles in the chipping mechanics. Here we shall generalize the earlier analysis of Eq. 1 by subsuming both θ and ϕ variations within a modified coefficient β, using an extension of the geometrical similarity principle. Of the two configurations in Fig. 1, the second is somewhat more restricted practically, at least in the case of sharp indenters with half-angle ψ, because of the geometrical constraint that point contacts can be made only within the range $\phi < \pi/2 - \psi$. In the case of a Vickers indenter, this means confinement to within $-16^\circ < \phi < 16^\circ$. Accordingly, we shall confine experimental validation of our extended analysis to non-orthogonal specimens in Fig. 1a, using the same normal Vickers indentations on transparent glass blocks as before but now with inclined edge faces.

2 Modified fracture mechanics

Consider a sharp, fixed-profile indenter making a contact at angle ϕ with the surface normal at a

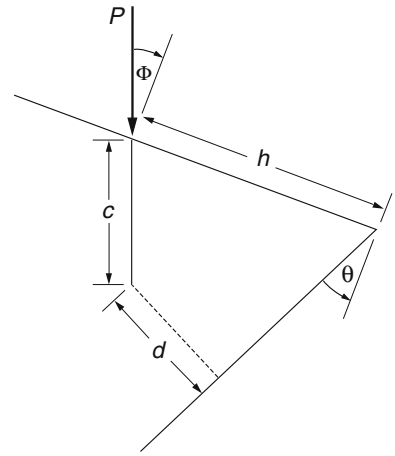

Fig. 2 Coordinate system for specimen with inclined side face in off-axis loading. Crack initially propagates downward along loading axis. At increasing depth c, crack begins to senses adjacent wall distant d away, and becomes unstable

distance h from the edge of a block with side face at angle θ to vertical. Define these angles as positive as shown in Fig. 2. The load axis is contained within a plane perpendicular to the specimen edge. The "point" contact generates a plastic zone which in turn generates a median crack. Allow the median crack to propagate with increasing load P through a distance c. Initially, the propagation is assumed to remain coplanar with the P vector, regardless of ϕ, consistent with a simple realignment of the Bousinesq-like point-load stress field along the load axis (Swain 1979). Once formed, the crack is driven downward by a crack-mouth wedging force. Subsequently, as it begins to sense the side wall, the crack curves outward into a classical spalling chip configuration. In conformity with geometrical similarity, we suppose that the point of instability occurs when the crack length c exceeds some fixed multiple of the perpendicular distance d of the crack tip from the side wall. Writing this critical distance as $c_F = \gamma d$, with coefficient γ independent of ϕ and θ, we have from straightforward geometry

$$\begin{aligned} c_F &= \gamma h \cos\theta/[1 + \gamma \sin(\phi + \theta)] \\ &= c_0 \cos\theta/[1 + \gamma \sin(\phi + \theta)] \end{aligned} \tag{2}$$

with $\gamma h = c_0$.

Now consider the corresponding critical loads. In our previous analysis we argued that the size of the propagating crack is related to the contact load by $P/c^{3/2} = (K_c/\chi_e) f(c/h)$, with $f(c/h)$ a dimensionless shape function representing the influence of the

side walls and χ_e a contact coefficient (Chai and Lawn 2007). At instability, $P = P_F$ at $c = c_F$, this reduces to

$$P_F/h^{3/2} = (K_c/\chi_e)(c_F/h)^{3/2} f(c_F/h) \quad (3)$$

If we now assert that the quantity $f(c_F/h)$ be insensitive to angular variation, we may combine Eqs. 2 and 3 to obtain a relation of analogous form to Eq. 1

$$\begin{aligned} P_F &= \beta K_c h^{3/2} \\ &= \beta_0 K_c h^{3/2} \{\cos\theta/[1+\gamma\sin(\phi+\theta)]\}^{3/2} \\ &= P_0 \{\cos\theta/[1+\gamma\sin(\phi+\theta)]\}^{3/2} \end{aligned} \quad (4)$$

with $\beta_0 = (1/\chi_e)\gamma^{3/2} f(c_0/h)$ and $P_0 = \beta_0 K_c h^{3/2}$ (Chai and Lawn 2007).

Beyond the instability point, the crack propagates to the side face to form the chip. Let the dimensions of the chip measured on that face be C and D, as defined in Fig. 1. We suppose that the projection $C/\cos(\phi+\theta)$ of the chip depth onto the line of action of the applied load will scale directly with c_F, and that D will scale with C. Then in conjunction with Eq. 2 we obtain

$$C = \gamma' h \cos\theta/\{\cos(\phi+\theta)[1+\gamma\sin(\phi+\theta)]\} \quad (5a)$$

$$D = \gamma'' h \cos\theta/\{cos(\phi+\theta)[1+\gamma\sin(\phi+\theta)]\} \quad (5b)$$

where $\gamma' h = C_0$ and $\gamma'' h = D_0$, with γ' and γ'' coefficients. The chip volume has the form

$$V = \alpha C D d \quad (6)$$

with α another coefficient. Note that V scales with h^3.

3 Experimental validation

3.1 Materials and methods

Model soda-lime glass specimens were fabricated from polished blocks of minimum dimension 12 mm. Glass was chosen so that the entire crack evolution could be followed with a video camera. One side face of each block was ground and polished to 1 μm finish with diamond paste at a prescribed angle of inclination θ, as in Fig. 1a.

Indentations were made on the glass top surfaces with a Vickers diamond pyramid at prescribed distances h between 1 and 3 mm from the edge, in normal loading ($\phi = 0$). Face angles in the range $-30° < \theta < 60°$, within which well-defined chips are obtainable, were examined. No non-normal loading was pursued, for the reasons of geometrical constraint outlined in Sect. 1, plus the fact that a tangential load component tended to cause slippage at the contact. The load rate was fixed at about $1\,\mathrm{N\,s^{-1}}$, so that chipping occurred within 1–2 min. A video camera was used to view crack development from the side, and crack depth c along the load axis monitored as a function of increasing load P up to the critical value P_F for chipping (Fig. 2).

Chip dimensions C and D on the side faces were measured *post mortem* (Fig. 1). Chip volumes were determined by weighing the specimen before and after indentation, using a value $2470\,\mathrm{kg/m^3}$ for the density of soda-lime glass.

3.2 Crack morphology

The basic geometrical elements of chip formation were more or less as before (Chai and Lawn 2007), but with elongation or foreshortening at different angles. Figure 3 shows three side views for each of three face inclinations, (a) $\theta = -20°$, (b) $+20°$, and (c) $+50°$, indicating the crack evolution to unstable chip formation. In each case the crack starts downward closely parallel to the loading axis. Then, at a critical depth, it begins to sense the adjacent face, and curves around into an unstable configuration to form a chip on the side wall. At the largest angle θ, Fig. 3c, the crack actually deviates a little away from the side wall before jumping into the chip formation. *Post-mortem* examination of the chipped faces showed the same scallop-shaped geometry as reported previously (Chai and Lawn 2007).

3.3 Crack evolution and critical loads

Data for the reduced critical chipping load quantity $P_F/h^{3/2}$ are plotted in Fig. 4 as a function of sidewall inclination θ for indentation distances h between 1 and 3 mm in normal loading. The unfilled symbol at $\theta = 0$ is the mean and standard deviation (20 tests) from the preceding study on rectangular specimens (Chai and Lawn 2007). The solid line is a prediction from Eq. 4 using best-fit parameters $\beta_0 = 9.3$ along with $K_c = 0.6\,\mathrm{MPa\,m^{1/2}}$ for soda-lime glass from the same preceding study, along with $\gamma = 1.5$. (This last parameter differs slightly from $\gamma = 2.0$ estimated in the preceding paper, but fits the broader range of angular data better.) The value of P_F diminishes with increasing θ, as may be expected. Of special note is the rapid

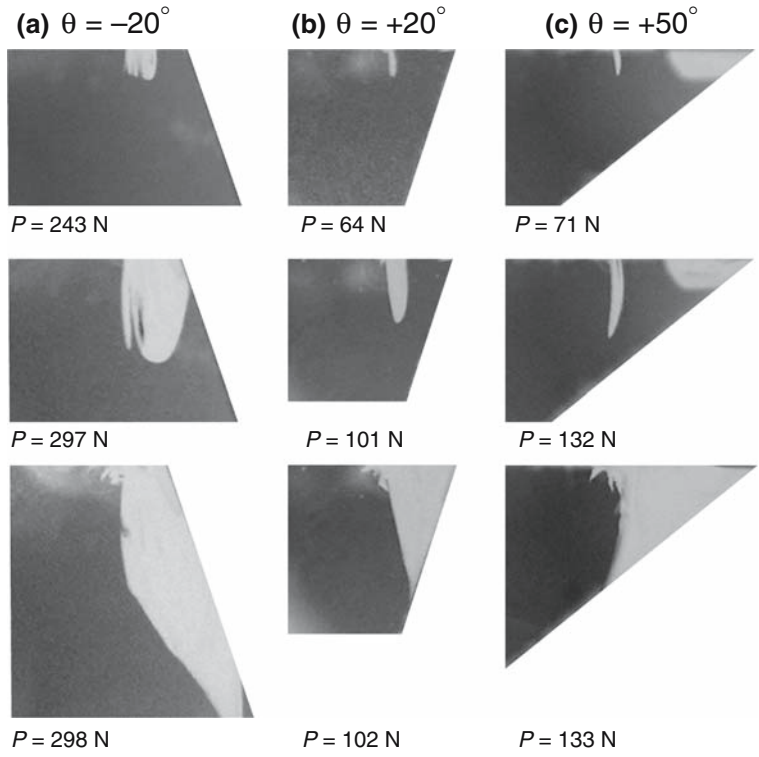

Fig. 3 Side views of Vickers cracks for normal loading ($\phi = 0$) on glass blocks with inclined side faces: (**a**) $\theta = -20°$, $h = 0.8$ mm; (**b**) $\theta = +20°$, $h = 1.0$ mm; (**c**) $\theta = +50°$, $h = 2.2$ mm

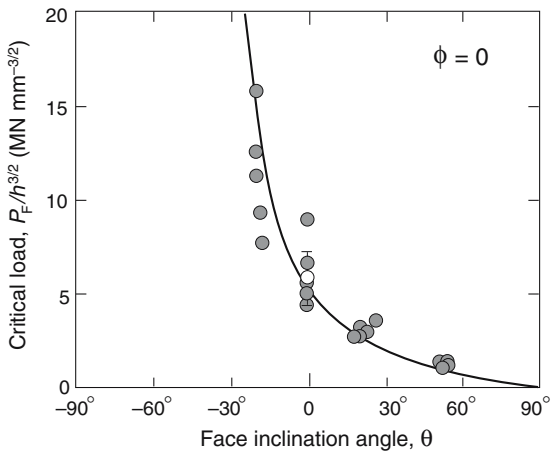

Fig. 4 Critical load $P_F/h^{3/2}$ versus side-face inclination angle θ for normal loading of Vickers indenter on glass blocks with inclined faces. Data for various indent location h. Solid curve is theoretical fit of Eq. 4

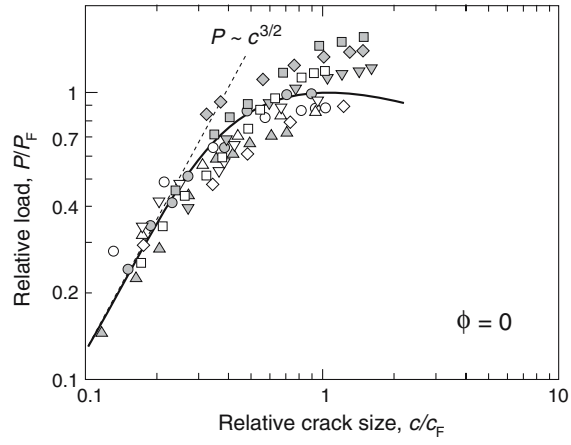

Fig. 5 Normalized load P/P_F on Vickers indenter as function of normalized crack size c/c_F. Each symbol represents data for a specific combination of θ and h, normal loading. Solid curve is empirical fit to data

rise at the other end of the angle scale, at $\theta < -30°$, indicating that heavily beveled edges may be immune to spalling.

Figure 5 shows more detailed information on crack evolution from in situ observations in the same specimens. Each symbol represents a different combination of h and θ, covering the same range of inclination angle ($-20° \leq \theta \leq +55°$) and indentation location ($1\,\text{mm} \leq h \leq 3\,\text{mm}$) as in Fig. 4. The data are normalized as P/P_F versus c/c_F, with P_F and c_F

computed from Eqs. 4 and 2, respectively, using $\gamma = 1.5$. Such a plot reduces all data to a single universal function, within the data scatter, drawn empirically as the solid curve. This curve passes through a maximum at $c = c_F$, corresponding to critical load instability at $P = P_F$. Note that some data in this plot extend beyond the instability point at $c = c_F$, attributable to slow crack growth effects from intrusion of water (Marshall et al. 1979). The curve is asymptotic to the inclined dashed line representing the limiting case $P \sim c^{3/2}$ for small cracks ($c << h$), corresponding to $f(c/h) = 1$ in Eq. 4 (Chai and Lawn 2007).

The fact that the data in Figs. 4 and 5 can be fitted, within scatter, to universal functions may be considered validation of the geometrical similarity principle.

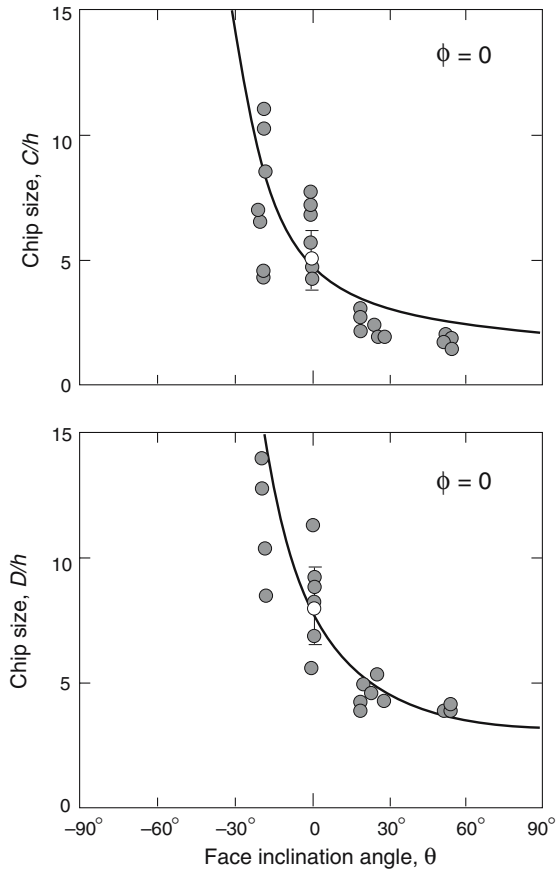

Fig. 6 Plots of relative chip dimensions C/h and D/h versus side-face inclination angle θ, normal loading. Data for various h. Unfilled symbols from previous study on rectangular specimens. Solid curves are theoretical fits of Eq. 5

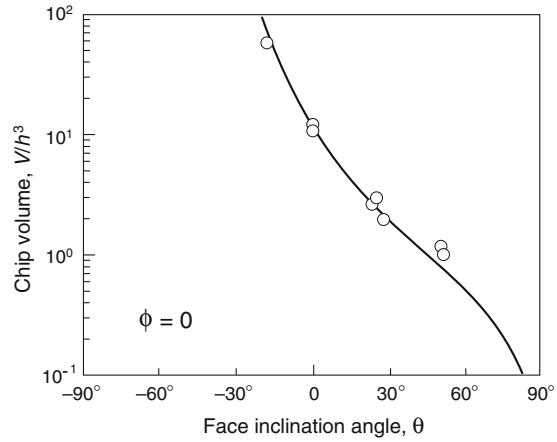

Fig. 7 Volume of chip as function of side-face angle θ, showing experimental data and prediction from Eq. 6

3.4 Chip dimensions

Plots of relative chip dimensions C/h and D/h are shown as a function of side-face inclination θ, again for normal loading, in Fig. 6. Filled symbols are data for indentation locations within the range $1\,\text{mm} \leq h \leq 3\,\text{mm}$. Unfilled symbols at $C_0/h = 5.1$ and $D_0/h = 8.0$ at $\theta = 0$ are means and standard deviations (20 tests) from the preceding study (Chai and Lawn 2007). Again, the data can be plotted on universal curves, within the scatter. Solid lines are theoretical fits from Eq. 5, using $\gamma' = C_0/h = 5.1$ and $\gamma'' = D_0/h = 8.0$. A rapidly diminishing chip size for increasing θ is apparent.

Figure 7 is a plot of reduced chip volume V/h^3 as a function of face angle θ. Data are from experimental measurements. The solid curve is a prediction using Eqs. 5 and 6, with the adjustment $\alpha = 0.32$. Noting the logarithmic ordinate, a strong falloff in V with increasing θ is apparent.

4 Discussion

In this study we have demonstrated the role of angular components in the chipping mechanics of brittle structures. An analytical description, based on geometrical similarity principles, has been developed for the general case of a point load delivered at angle ϕ with the surface normal at a distance h from the edge of a block with side face at angle θ to orthogonal. The analysis retains the explicit relation $P_F = \beta K_c h^{3/2}$ in

Eq. 1 for the critical chipping load P_F in terms of indent location h and toughness K_c, with the angular dependence conveniently incorporated into the coefficient β. Experimental validation has been given for Vickers indentations loaded normally ($\phi = 0$) onto glass blocks with inclined side faces ($\theta \neq 0$). The critical loads P_F diminish strongly with increasing angle θ, as seen in Fig. 4. Of special interest in Fig. 4 are the responses at each end of the angle range: at large θ (flakes), P_F is relatively small, accounting in part for the ease of chip formation in stone tools (Dibble and Pelcin 1995); at small negative θ (chamfers), P_F is prohibitively high, explaining the immunity of properly beveled edges to visible damage. The chip dimensions (Figs. 6 and 7) also diminish strongly with increasing θ (positive angle defined as in Figs. 1 and 2), i.e., consistent with an ever-increasing free-surface influence. Equation 4 predicts a similar trend with increasing load angle ϕ, but this dependence was not investigated here.

There are acknowledged limitations in the present study. In the analysis of Sect. 2 it was assumed that the notion of geometrical similarity universally extends to all angles θ and ϕ, including the function $f(c_F/h)$ in Eq. 3. Such "universality" is not based on rigorous fracture mechanics. However, the "goodness" of the data fits in Figs. 4–7 suggests that our assumption is a reasonable approximation, at least for the θ dependence, within the scatter. Experimentally, we have restricted our consideration to just one indenter type, a Vickers pyramid, with its attendant constraints on load-axis angle ($-16° < \phi < 16°$). Recall that it is this constraint which has precluded a study of off-axis loading here, which leaves validation (or otherwise) of the ϕ dependence as an outstanding issue. In reality, since the well-developed median crack is driven by a mouth-wedging force exerted by the walls of the indenter, the quantity β_0 must also be a function of indenter angle ψ (Fig. 1) (Lawn and Fuller 1975), which means that Eq. 4 should strictly be recalibrated for each indenter type. Intuitively, use of a sharper indenter (smaller ψ) must be expected to diminish the critical load for chipping; and, at the same time, to lessen the constraint on the load axis (larger allowable range in ϕ). Proceeding in the opposite direction to blunter indenters, typified by spheres, may add extra complications, for instance by generating altogether different fracture geometries (cone cracks). The role of indenter geometry is a factor that warrants further investigation.

Notwithstanding these limitations, Eq. 4 has a certain power. It conveniently expresses the spatial and angular coordinates in separable terms. Thus, for any given indenter, one need only measure the critical quantity P_0 from control tests at $\theta = 0 = \phi$ in order to predict P_F for any specimen and loading configuration. Thus tests for any specific indenter could be conducted on rectangular specimens in normal loading to evaluate $P_0/h^{3/2}$ in Eq. 4, from which values of P_F for any combination of θ and ϕ could be predetermined, even if K_c were not known a priori.

A condition for applicability of Eq. 4 is that a chip always forms on the side face. There are some cases where this condition may not be met. Where the characteristic depth C becomes sufficiently large, especially in the region $\theta << 0$ or $\phi << 0$, the chip may extend through the specimen to the bottom rather than side face. In such cases, specimen size becomes an issue. Conversely, where C becomes vanishingly small, at $\theta >> 0$ or $\phi >> 0$, or at $h >> 0$, the chip may emerge on the top surface. Such limiting cases, while perhaps of interest in some applications (e.g., stone tool flaking (Dibble and Pelcin 1995)), lie beyond the scope of the present work.

As in the preceding study (Chai and Lawn 2007), there are additional factors that could be issues in chip formation. These include: rate effects from the intrusion of ambient moisture into the cracks, accelerating crack growth in prolonged loading states; R-curves in brittle materials with heterogeneous microstructures, in which case the assumption of a single-valued toughness K_c in Eq. 4 breaks down; more complex edge geometry, e.g., rounded corners; indenter geometry effects and additional fracture modes, especially in transitions to very sharp or very blunt indenters; in off-axis loading, potential slippage and friction at the contact point, leading to multiple cracking. Application of the fracture mechanics relations in Sect. 2 needs to be made with due recognition of these and any other influencing factors.

Acknowledgements This work was supported by a grant from the U.S. National Institute of Dental and Craniofacial Research (PO1 DE10976).

Certain equipment, instruments or materials are identified in this paper to specify experimental details. Such identification does not imply recommendation by the National Institute of Standards and Technology, nor does it imply that the materials are necessarily the best available for the purpose.

References

Almond EA, McCormick NJ (1986) Constant-geometry edge flaking of brittle materials. Nature 321:53–55

Chai H, Lawn BR (2007) A universal relation for edge chipping from sharp contacts in brittle materials: a simple means of toughness evaluation. Acta Mater 55:2555–2561

Chui WC, Thouless MD, Endres WJ (1998) An analysis of chipping in brittle materials. Int J Fract 90:287–298

Cotterell B, Kaminga J, Dickson FP (1985) The essential mechanics of conchoidal flaking. Int J Fract 29:205–221

Dibble HL, Pelcin A (1995) The effect of hammer mass and velocity on flake mass. J Archaeol Sci 22:429–439

Lardner TJ, Ritter JE, Shiao ML, Lin MR (1990) Behavior of indentation cracks near free surfaces and interfaces. Int J Fract 44:133–143

Lawn BR, Fuller ER (1975) Equilibrium penny-like cracks in indentation fracture. J Mater Sci 10:2016–2024

Marshall DB, Lawn BR, Chantikul P (1979) Residual stress effects in sharp-contact cracking: II. Strength degradation. J Mater Sci 14:2225–2235

McCormick NJ (1982) Edge flaking as a measure of material performance. Met Mater 8:154

Morrell R (2005) Edge flaking—similarity between quasistatic indentation and impact mechanisms for brittle materials. Key Eng Mater 290:14–22

Morrell R, Gant AJ (2001) Edge chipping of hard materials. Int J Refract Met Hard Mater 19:293–301

Quinn JB, Su L, Flanders L, Lloyd IK (2000) 'Edge toughness' and material properties related to the machining of dental ceramics. Mach Sci Technol 4:291–304

Scieszka SC (2005) Edge failure as a means of concurrently estimating the abrasion and edge fracture resistance of hard metals. Tribol Int 38:834–842

Swain MV (1979) Microfracture about scratches in brittle solids. Proc Roy Soc Lond A A366:575–597

Thouless MD, Evans AG, Ashby MF, Hutchinson JW (1987) The edge cracking and spallation of brittle plates. Acta Metall 35:1333–1341